ARTICLES

Particle ratios of high-x_t hadrons in p-A interactions at $\sqrt{s} = 38.8$ GeV

P.B. Straub,[ι] D.E. Jaffe,[θ(a)] H.D. Glass,[θ(b)] M.R. Adams,[θ(c)] C.N. Brown,[δ] G. Charpak,[β] W.E. Cooper,[δ] J.A. Crittenden,[γ(d)] D.A. Finley,[δ] R. Gray,[ι(e)] Y. Hemmi,[η] Y.B. Hsiung,[γ(b)] J.R. Hubbard,[α] A.M. Jonckheere,[δ] H. Jöstlein,[δ] D.M. Kaplan,[ε(f)] L.M. Lederman,[δ(g)] K.B. Luk,[ι(h)] A. Maki,[ζ] Ph. Mangeot,[α] R.L. McCarthy,[θ] K. Miyake,[η] R.E. Plaag,[i(i)] J.P. Rutherfoord,[ι(j)] Y. Sakai,[ζ] J.C. Santiard,[β] F. Sauli,[β] S.R. Smith,[γ(k)] T. Yoshida,[η(l)] and K.K. Young,[ι]

[α] *Centre d'Etudes Nucléaires de Saclay, Gif-sur-Yvette, 91190 France*
[β] *CERN, CH-1124 Geneva, 23 Switzerland*
[γ] *Columbia University, New York, New York 10027*
[δ] *Fermi National Acceleration Laboratory, Batavia, Illinois 60510*
[ε] *Florida State University, Tallahassee, Florida 32306*
[ζ] *KEK, Tsukuba, Ibaraki-ken, 305 Japan*
[η] *Kyoto University, Kyoto, 606 Japan*
[θ] *State University of New York, Stony Brook, New York 11794*
[ι] *University of Washington, Seattle, Washington 98195*

(Received 27 December 1990)

We report measurements of the ratios K^+/π^+, p/π^+, K^-/π^-, $\bar{p}/\pi^-$, π^-/π^+, K^-/K^+, and $\bar{p}/p$ for hadrons with $0.19 < x_t < 0.62$ produced in p-Be and p-W collisions at $\sqrt{s} = 38.8$ GeV. The K^+/π^+ ratio at high x_t gives the fragmentation-function ratio $D_u^{K^+}/D_u^{\pi^+}$ at high z. The high-x_t K^-/π^- ratio gives an upper limit for $D_d^{K^-}/D_d^{\pi^-}$ at high z. The p_t dependence of p/π^+ suggests that scattered constituent diquarks are the primary source of protons with $p_t < 6$ GeV/c. We also present species correlations in high-mass h^+h^- pairs. Strong K^+K^- and $p\bar{p}$ correlations were observed.

PACS number(s): 13.85.Ni, 13.87.Fh, 25.40.Ve

I. INTRODUCTION

Hadronization is most cleanly studied in e^+e^- annihilation, but existing results on identified hadrons [1] extend only to 0.8 in $z = p_{\text{hadron}}/p_{\text{jet}}$. In contrast, hadrons produced in p-p collisions with high $x_t = 2p_t/\sqrt{s}$ have very high average z. For π^0 production at $\sqrt{s}$ between 31 and 62 GeV, the average z increases roughly linearly from 0.83 to 0.92 as x_t increases from 0.17 to 0.42 [2]. Fragmentation of quarks and gluons is typically described by a fragmentation function $D_p^h(z)$ (defined as the probability density in z of hadrons of species h produced in the hadronization of a parton of species p). Particle ratios of high-x_t hadrons produced in hadronic collisions can constrain models of high-x_t parton production and also give unique data on fragmentation function ratios at high z, although the extraction of this information is model dependent.

Using the E605 spectrometer [3–5] at Fermilab, we have measured the particle ratios K^+/π^+, p/π^+, K^-/π^-, $\bar{p}/\pi^-$, π^-/π^+, K^-/K^+, and $\bar{p}/p$ with p_t between 3.6 and 12 GeV/c in collisions of 800-GeV protons with beryllium and tungsten nuclei. In addition, we have measured particle fractions and opposite-side species correlations for h^+h^- pairs with a mass between 8 and 15 GeV/c^2. The results on A dependence are given in a separate paper [5]. The E605 detector, a focusing pair spectrometer, simultaneously accepted positively and negatively charged particles produced at angles between 76° and 95° in the proton-nucleon center-of-momentum frame. For positive magnet polarity, ac-

[a] Laboratoire de l'Accélérateur Linéaire, 91405 Orsay, France.
[b] Present address: FNAL, Batavia, IL 60510.
[c] Present address: University of Illinois at Chicago, Chicago, IL 60680.
[d] Present address: Physikalisches Institut der Universität Bonn, Nussallee 12, 5300 Bonn 1, Federal Republic of Germany.
[e] Present address: University of Minnesota, Minneapolis, MN 55455.
[f] Present address: Northern Illinois University, Dekalb, IL 60115.
[g] Present Address: University of Chicago, Chicago, IL 60637.
[h] Present address: University of California at Berkeley, Berkeley, CA 94720.
[i] Present address: High Technology Center, Boeing Electronics Co., P.O. Box 24969, MS7J-56, Seattle, WA 98124-6269.
[j] Present address: University of Arizona, Tucson, AZ 85721.
[k] Present address: SLAC, Stanford, CA 94309.
[l] Present address: Osaka City University, Osaka 558, Japan.

cepted positively (negatively) charged particles passed over (under) the beam dump and were bent down (up) before entering the detector. This geometry allowed acceptance of h^+h^- pairs with azimuthal angles differing by more than 140°.

II. EXPERIMENTAL TECHNIQUE

Hadrons were identified with a ring imaging Cherenkov detector [6, 7]. The Cherenkov radiator gas, helium at ambient temperature and pressure, was contained in a 15-m-long aluminum tank. The index of refraction of the helium was typically 1.000 036, giving a threshold momentum of 111 GeV/c for protons. A 4 × 4 array of spherical mirrors with an 8 m focal length was suspended in the downstream end of the tank. They reflected Cherenkov light onto two multistep proportional chambers [8, 9] which were used to reconstruct the photon positions to an accuracy of 0.3 mm. The photon pattern recognition was done by matching amplitudes between the anode plane and the two cathode planes. The radius of the Cherenkov ring for a high-momentum track was typically 70 mm, smeared by 0.7 mm due to the chromatic dispersion of the radiator gas. For each run (runs lasted about one hour), samples of high-momentum muons were used to determine the orientation of each mirror, the index of refraction, and the chromatic dispersion of the helium. An average of 2.5 Cherenkov photons were detected for high-momentum tracks, accompanied by 1.0 noise photons within 85 mm of the ring center. Figure 1 shows the distribution in reconstructed ring-radii and track momentum for tracks which had exactly one reconstructed photon.

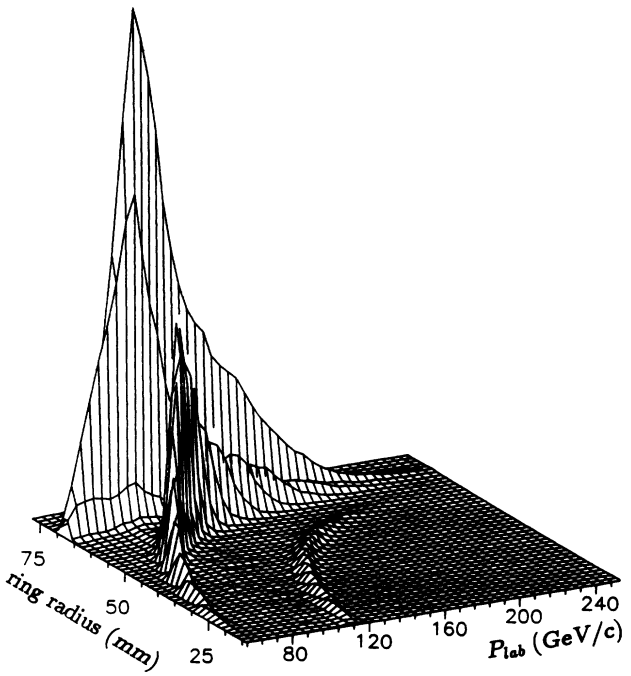

FIG. 1. Distribution in measured photon-ring-radius and track momentum for single-photon events.

For each track we calculated the likelihood L^α ($\alpha = \pi$, K, or p) for each species to produce the reconstructed photon pattern [10]. For a sample of N_t tracks, these per-track likelihoods were used to estimate the particle fractions f_α for each of the three hadron species by solving the likelihood equations

$$f_\alpha = \frac{1}{N_t}\sum_{i=1}^{N_t}\frac{L_i^\alpha f_\alpha}{\sum_\beta L_i^\beta f_\beta}. \tag{1}$$

The per-track likelihoods L^α were calculated in terms of the estimated number-of-photon and photon-position distributions for Cherenkov and noise photons. For Cherenkov photons, under species hypothesis α, $P_{\rm Ch}^\alpha(k)$ designates the probability for k Cherenkov photons to be reconstructed and $\rho_{\rm Ch}^\alpha(\mathbf{s})$ is the probability density for a Cherenkov photon to be reconstructed at position $\mathbf{s}$. The corresponding distributions for noise photons are $P_{\rm noise}$ and $\rho_{\rm noise}$. For a single-track event with N photons reconstructed at positions $\mathbf{s}_1$ through $\mathbf{s}_N$, L^α is a probability density over the N photon positions. The density is written as a sum over 2^N terms corresponding to the possible interpretations of each photon as signal or noise:

$$L^\alpha(\mathbf{s}_1\cdots\mathbf{s}_N)=\sum_{i_1=0}^{1}\cdots\sum_{i_N=0}^{1}\frac{P_{\rm Ch}^\alpha(N_{\rm Ch})P_{\rm noise}(N-N_{\rm Ch})}{\binom{N}{N_{\rm Ch}}}\prod_{k=1}^{N}\begin{cases}\rho_{\rm noise}(\mathbf{s}_k), & i_k=0,\\ \rho_{\rm Ch}^\alpha(\mathbf{s}_k), & i_k=1.\end{cases} \tag{2}$$

The index i_k set to zero or one corresponds to photon k being interpreted as noise or signal. For each term, the number of Cherenkov photons, $N_{\rm Ch}$, is equal to the number of nonzero i_k's.

The analysis for h^+h^- pair events was a straightforward extension of the procedure for single hadrons. For each pair event, nine per-event likelihoods $L^{\alpha\beta}$ were computed. For a sample of N_p pair events, the pair fractions $f_{\alpha\beta}$ (α labels the positive hadron species and β the negative) were obtained by solving the likelihood equations

$$f_{\alpha\beta} = \frac{1}{N_p}\sum_{i=1}^{N_p}\frac{L_i^{\alpha\beta} f_{\alpha\beta}}{\sum_{\mu\nu} L_i^{\mu\nu} f_{\mu\nu}}. \tag{3}$$

The per-event likelihoods were computed as

$$L^{\alpha\beta}(\mathbf{s}_1\cdots\mathbf{s}_N)=\sum_{i_1=0}^{2}\cdots\sum_{i_N=0}^{2}\frac{P_{\rm Ch}^{\alpha\beta}(N_{\rm Ch})P_{\rm noise}(N-N_{\rm Ch})}{\binom{N}{N_{\rm Ch}}\binom{N_{\rm Ch}}{N_{\rm Ch,1}}}\prod_{k=1}^{N}\begin{cases}\rho_{\rm noise}(\mathbf{s}_k), & i_k=0,\\ \rho_{\rm Ch}^{\alpha,1}(\mathbf{s}_k), & i_k=1,\\ \rho_{\rm Ch}^{\beta,2}(\mathbf{s}_k), & i_k=2.\end{cases} \tag{4}$$

In calculating $L^{\alpha\beta}$, each photon had three possible interpretations: $i_k = 0$ for noise photons and $i_k = 1$ or 2 for Cherenkov photons from track 1 or track 2. The number-of-photon distributions $P_{\rm Ch}^{\alpha\beta}$ and $P_{\rm noise}$ were computed for the pair. Position probability densities $\rho_{\rm Ch}^{\alpha,1}(\mathbf{s})$ and $\rho_{\rm Ch}^{\beta,2}(\mathbf{s})$ were computed for each track.

Samples of single-muon and muon-pair events were used to tabulate number-of-photon distributions for each run. These distributions were used to estimate $P_{\rm Ch}$ and $P_{\rm noise}$ for each single-hadron or hadron-pair event, taking into account the track momentum, the photon acceptance, and the merging of photons due to confusion in the pattern recognition. Because of fluctuating detector efficiency, the number-of-photon distributions were poorly described by Poisson statistics.

The position probability density $\rho_{\rm Ch}^{\alpha}(\mathbf{s})$ for Cherenkov photons from a particular track was described by a Gaussian in the difference between the reconstructed and calculated ring radii. The width of this Gaussian was calculated by adding in quadrature errors in the radius due to chromatic dispersion, detector resolution, astigmatism, and uncertainties in the mirror orientation and the track momentum. The noise photons were described by a uniform distribution in position [i.e., $\rho_{\rm noise}(\mathbf{s})$ was a constant function].

The particle fractions obtained from Eqs. (1) and (3) were corrected for decays and absorption in the detector. In the lowest p_t bins the correction for decays was as high as 11% for kaons and 1.5% for pions. For each track, the probability for absorption in the apparatus was computed. Typical values were 2% for pions and kaons and 3% for protons and antiprotons [11].

For $p_t < 6$ GeV/c, most tracks were near or below the Cherenkov threshold for protons, so the determination of the proton and antiproton fractions was largely a subtractive measurement. Accurate estimation of $P_{\rm Ch}^{\pi}(0)$ and $P_{\rm Ch}^{K}(0)$, the probabilities for pions and kaons to produce zero photons, was essential. The sensitivity of the particle ratios to errors in the per-track number-of-photon distributions $P_{\rm Ch}^{\alpha}$ was estimated by reanalyzing the data using distributions which had been modified so that the mean number of photons was 10% higher or lower. The systematic errors given in the tables reflect these variations (all tables show statistical, then systematic errors). The errors quoted in the text and the error bars in the plots which follow give the statistical errors added in quadrature with these systematic variations.

Unlike the same-charge particle ratios, the ratios π^-/π^+, K^-/K^+, and $\bar{p}/p$ depended not only on Cherenkov detector measurements, but also on the h^-/h^+ ratio which was determined by comparing two data sets taken with opposite magnet polarity. This resulted in two independent measurements of h^-/h^+ for each p_t bin, one using tracks which passed through the upper aperture and the other using lower aperture tracks. In this way the samples of positive and negative hadrons being compared had identical geometric acceptance and reconstruction efficiencies which differed only due to temporal variations [10,5]. The h^-/h^+ ratios for each p_t bin were determined using a maximum-likelihood fit which also determined the error in the ratio of luminosities between the positive and negative magnet polarity data sets. This procedure has the advantage that, to first order, it is insensitive to luminosity measurement errors.

III. SAME-CHARGE PARTICLE RATIOS FOR HIGH-p_t HADRONS

Figure 2 and Table I show the ratio K^+/π^+ for hadrons produced in p-Be and p-W collisions. In p-Be the ratio shows very little p_t dependence, decreasing from 0.50 ± 0.01 at p_t of 3.9 GeV/c to 0.48 ± 0.01 for $p_t > 7$ GeV/c. For p-W, the same ratio falls from 0.55 ± 0.01 at p_t of 3.9 GeV/c to 0.50 ± 0.01 for $p_t > 7$ GeV/c. The slightly larger ratio K^+/π^+ observed in p-W interactions near p_t of 4 GeV/c could be explained by increased production of high-p_t gluons in large nuclei [5] together with enhanced strangeness production in gluon fragmentation. At high x_t, where gluon fragmentation and resonance decay are not significant sources of kaons or pions, the ratio K^+/π^+ directly measures the fragmentation function ratio $D_u^{K^+}/D_u^{\pi^+}$, which is the relative probability for a u quark to bind with an $\bar{s}$ or a $\bar{d}$ at high z. As p_t increases from 4.2 GeV/c to 10.2 GeV/c, we estimate that the fraction of K^+'s coming from gluon fragmentation drops from 50% to 6% in p-Be (see Sec. IV).

For $x_t > 0.2$ the 400-GeV Chicago-Princeton [12] (CP) K^+/π^+ data are compatible with our results. In p-p collisions the K^+/π^+ ratio at high x_t has been measured to be 0.44 ± 0.01 at $\sqrt{s} = 27.4$ GeV [13], 0.48 ± 0.01 at $\sqrt{s} = 38.8$ GeV [4], 0.45 ± 0.02 at $\sqrt{s} = 45$ GeV [14],

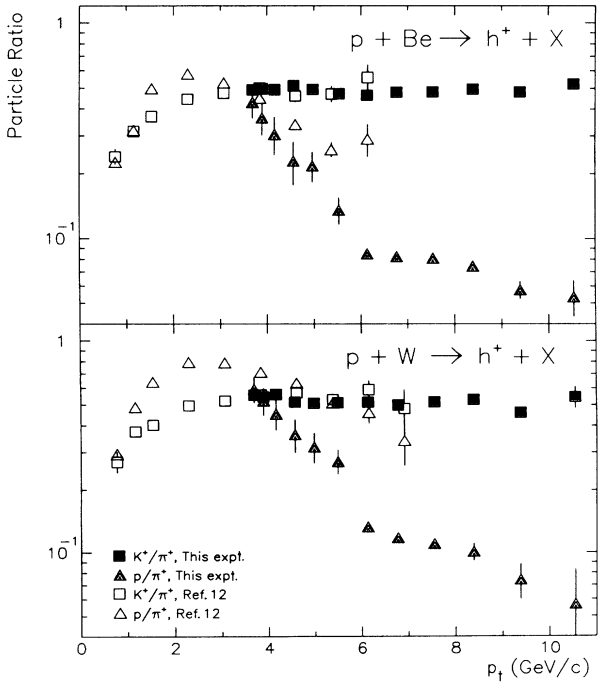

FIG. 2. Ratios K^+/π^+ (squares) and p/π^+ (triangles) vs p_t for hadrons produced in p-Be (above) and p-W (below) collisions. Open symbols are Chicago-Princeton data with $\sqrt{s}$=27.4 GeV/c.

TABLE I. K^+/π^+ ratio vs p_t in p+Be and p+W collisions.

p_t range (GeV/c)		$< p_t >$ (GeV/c)	p+Be K^+/π^+	$< p_t >$ (GeV/c)	p+W K^+/π^+
3.6	3.8	3.70	$0.491 \pm 0.005 \pm 0.008$	3.71	$0.557 \pm 0.013 \pm 0.010$
3.8	4.0	3.90	$0.496 \pm 0.004 \pm 0.008$	3.90	$0.545 \pm 0.010 \pm 0.010$
4.0	4.4	4.17	$0.492 \pm 0.003 \pm 0.008$	4.17	$0.561 \pm 0.008 \pm 0.010$
4.4	4.8	4.57	$0.512 \pm 0.005 \pm 0.005$	4.57	$0.514 \pm 0.012 \pm 0.007$
4.8	5.2	4.98	$0.494 \pm 0.007 \pm 0.002$	4.98	$0.509 \pm 0.017 \pm 0.004$
5.2	5.8	5.54	$0.471 \pm 0.008 \pm 0.000$	5.49	$0.512 \pm 0.022 \pm 0.001$
5.8	6.4	6.14	$0.464 \pm 0.004 \pm 0.001$	6.13	$0.515 \pm 0.010 \pm 0.002$
6.4	7.2	6.77	$0.479 \pm 0.003 \pm 0.001$	6.77	$0.500 \pm 0.008 \pm 0.002$
7.2	8.0	7.54	$0.481 \pm 0.004 \pm 0.001$	7.55	$0.515 \pm 0.011 \pm 0.002$
8.0	9.0	8.39	$0.495 \pm 0.007 \pm 0.002$	8.38	$0.529 \pm 0.017 \pm 0.002$
9.0	10.0	9.40	$0.480 \pm 0.012 \pm 0.003$	9.38	$0.460 \pm 0.030 \pm 0.002$
10.0	13.0	10.53	$0.524 \pm 0.024 \pm 0.002$	10.55	$0.545 \pm 0.063 \pm 0.002$

and 0.46 ± 0.02 at $\sqrt{s} = 62$ GeV [14], (these numbers are weighted averages of all data points with $x_t > 0.2$).

Figure 2 and Table II show the ratio p/π^+ for hadrons produced in p-Be and p-W collisions. In p-Be, p/π^+ drops from 0.43 ± 0.07 to 0.085 ± 0.005 as p_t increases from 3.7 to 6.1 GeV/c. In p-W, the p/π^+ ratio also drops, from 0.59 ± 0.09 to 0.13 ± 0.01 over the same interval. At higher p_t, the p/π^+ curve is much flatter for both targets, decreasing to about 0.06 at p_t of 10 GeV/c. A rapid drop of p/π^+ with p_t, followed by a high-p_t flattening is expected in a model in which scattered pointlike diquarks are a source of high-p_t protons [15,16,4]. The rapid drop with p_t of p/π^+ for p_t below 6 GeV/c reflects the Q^2 dependence of the diquark form factor. For p_t above 6 GeV/c scattered u quarks become the dominant source of protons and the p_t dependence of p/π^+ reflects the z dependence of $D_u^p/D_u^{\pi^+}$. A comparison with the CP data [12] indicates that the ratio p/π^+ drops with $\sqrt{s}$ at fixed p_t (fixed Q^2).

Figure 3 shows the ratios K^-/π^- and $\bar{p}/\pi^-$. The corresponding data are given in Tables III and IV. Since K^-'s and $\bar{p}$'s have no valence quarks in common with protons and neutrons, they must be produced by scattered gluons or sea quarks, or by rank reordering (i.e., the leading quark does not appear in the leading hadron). The steady decline of K^-/π^- and $\bar{p}/\pi^-$ with increasing p_t indicate the decreasing importance of these mechanisms compared to d-quark scattering. If we ignore sea quarks and make the reasonable assumption that K^-/π^- is larger in gluon and u-quark jets than in d-quark jets, then the measured K^-/π^- at high x_t is an upper limit for the fragmentation function ratio $D_d^{K^-}/D_d^{\pi^-}$ at high z. In p-Be interactions, for $p_t > 9$ GeV/c, which corresponds to an average z of about 0.92 (we estimate z using the results in Ref. [2]), that upper limit is 0.044 ± 0.006. Using similar logic, the $\bar{p}/\pi^-$ ratio in p-Be interactions with $p_t > 8$ GeV/c of 0.0017 ± 0.0007 gives the upper limit of the fragmentation function ratio $D_{\bar{d}}^{\bar{p}}/D_d^{\pi^-}$ for $z \sim 0.90$.

IV. OPPOSITE-CHARGE PARTICLE RATIOS FOR HIGH-p_t HADRONS

Figure 4 shows the ratios π^-/π^+, K^-/K^+, and $\bar{p}/p$. The π^-/π^+ ratio is given in Table V. The drop of π^-/π^+

TABLE II. p/π^+ ratio vs p_t in p+Be and p+W collisions.

p_t range (GeV/c)		$< p_t >$ (GeV/c)	p+Be p/π^+	$< p_t >$ (GeV/c)	p+W p/π^+
3.6	3.8	3.70	$0.429 \pm 0.005 \pm 0.067$	3.71	$0.592 \pm 0.013 \pm 0.080$
3.8	4.0	3.90	$0.364 \pm 0.004 \pm 0.062$	3.90	$0.522 \pm 0.010 \pm 0.076$
4.0	4.4	4.17	$0.305 \pm 0.003 \pm 0.061$	4.17	$0.453 \pm 0.008 \pm 0.073$
4.4	4.8	4.57	$0.229 \pm 0.004 \pm 0.052$	4.57	$0.362 \pm 0.011 \pm 0.063$
4.8	5.2	4.98	$0.217 \pm 0.006 \pm 0.034$	4.98	$0.317 \pm 0.016 \pm 0.049$
5.2	5.8	5.54	$0.136 \pm 0.006 \pm 0.018$	5.49	$0.272 \pm 0.019 \pm 0.029$
5.8	6.4	6.14	$0.085 \pm 0.002 \pm 0.003$	6.13	$0.132 \pm 0.006 \pm 0.005$
6.4	7.2	6.77	$0.082 \pm 0.001 \pm 0.002$	6.77	$0.117 \pm 0.005 \pm 0.004$
7.2	8.0	7.54	$0.081 \pm 0.002 \pm 0.002$	7.55	$0.110 \pm 0.006 \pm 0.003$
8.0	9.0	8.39	$0.074 \pm 0.003 \pm 0.001$	8.38	$0.101 \pm 0.009 \pm 0.003$
9.0	10.0	9.40	$0.058 \pm 0.005 \pm 0.001$	9.38	$0.074 \pm 0.014 \pm 0.001$
10.0	13.0	10.53	$0.053 \pm 0.010 \pm 0.001$	10.55	$0.057 \pm 0.026 \pm 0.001$

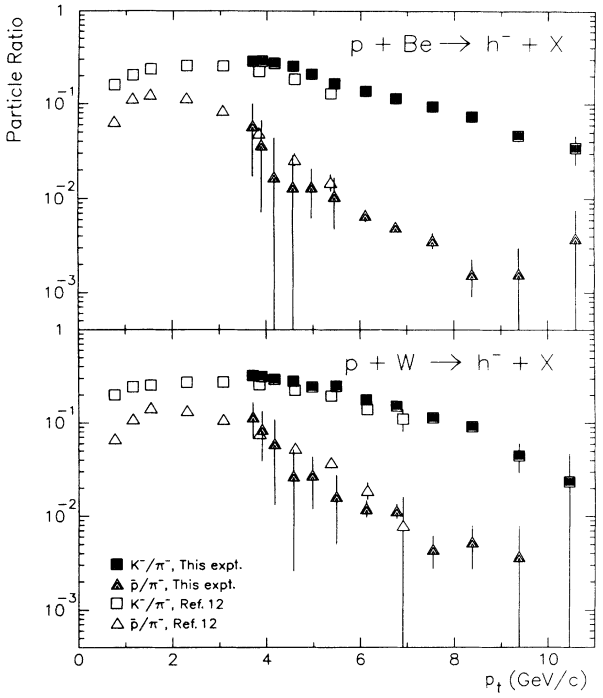

FIG. 3. Ratios K^-/π^- (squares) and $\overline{p}/\pi^-$ (triangles) vs p_t for hadrons produced in p-Be (above) and p-W (below) collisions. Open symbols are Chicago-Princeton data with $\sqrt{s}$=27.4 GeV/c.

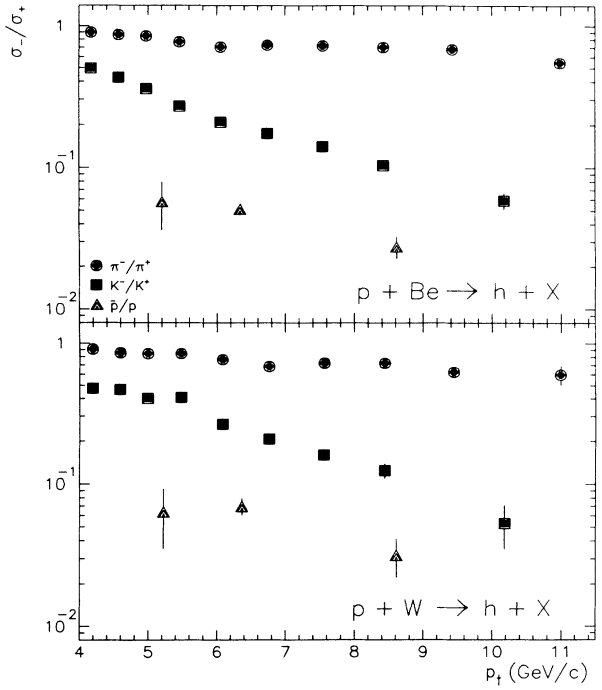

FIG. 4. Ratios π^-/π^+ (circles), K^-/K^+ (squares), and $\overline{p}/p$ (triangles) vs p_t for hadrons produced in p-Be (above) and p-W (below) collisions.

vs p_t reflects the drop with x of the d/u structure function ratio in the proton. The K^-/K^+ ratio (Table VI) falls much more steeply with increasing p_t because K^-'s, unlike K^+'s, have no valence quarks in common with the nucleons. If we assume that gluons are equally likely to fragment to K^+ or K^- and if we ignore rank reordering and sea quarks, K^-/K^+ gives the fraction of K^+'s of gluonic origin. Similarly, the ratio $\overline{p}/p$ (Table VII) gives an upper limit for the fraction of protons of gluonic origin, assuming that a gluon will equally likely fragment to a proton or an antiproton. The results show that, even at the lowest measured p_t values, only a small fraction of protons are of gluonic origin.

V. PARTICLE FRACTIONS FOR HIGH-MASS HADRON PAIRS

The particle fractions for h^+h^- pairs in two mass bins are given in Table VIII for the p-Be data and Table IX for the p-W data. The pair fractions were used to compute correlations between the opposite-side hadrons. The correlation $c_{\alpha\beta}$ between positive hadron species α and neg-

TABLE III. K^-/π^- ratio vs p_t in p+Be and p+W collisions.

p_t range (GeV/c)		$< p_t >$ (GeV/c)	p+Be K^-/π^-	$< p_t >$ (GeV/c)	p+W K^-/π^-
3.6	3.8	3.72	0.285 ± 0.005 ± 0.005	3.71	0.322 ± 0.010 ± 0.006
3.8	4.0	3.90	0.286 ± 0.003 ± 0.002	3.90	0.314 ± 0.008 ± 0.006
4.0	4.4	4.17	0.272 ± 0.003 ± 0.002	4.17	0.294 ± 0.006 ± 0.006
4.4	4.8	4.57	0.253 ± 0.004 ± 0.000	4.57	0.281 ± 0.009 ± 0.001
4.8	5.2	4.97	0.208 ± 0.005 ± 0.001	4.97	0.243 ± 0.013 ± 0.001
5.2	5.8	5.46	0.166 ± 0.006 ± 0.001	5.49	0.248 ± 0.016 ± 0.002
5.8	6.4	6.13	0.138 ± 0.003 ± 0.001	6.13	0.177 ± 0.007 ± 0.001
6.4	7.2	6.77	0.114 ± 0.002 ± 0.001	6.77	0.152 ± 0.005 ± 0.001
7.2	8.0	7.55	0.094 ± 0.003 ± 0.001	7.55	0.114 ± 0.007 ± 0.001
8.0	9.0	8.39	0.073 ± 0.004 ± 0.001	8.38	0.091 ± 0.010 ± 0.001
9.0	10.0	9.38	0.046 ± 0.006 ± 0.001	9.38	0.045 ± 0.016 ± 0.001
10.0	13.0	10.60	0.034 ± 0.012 ± 0.000	10.46	0.024 ± 0.024 ± 0.000

TABLE IV. $\bar{p}/\pi^-$ ratio vs p_t in p+Be and p+W collisions.

p_t range (GeV/c)		$< p_t >$ (GeV/c)	p+Be $\bar{p}/\pi^-$	$< p_t >$ (GeV/c)	p+W $\bar{p}/\pi^-$
3.6	3.8	3.72	$0.0587 \pm 0.0041 \pm 0.0415$	3.71	$0.1164 \pm 0.0094 \pm 0.0480$
3.8	4.0	3.90	$0.0369 \pm 0.0028 \pm 0.0296$	3.90	$0.0856 \pm 0.0068 \pm 0.0463$
4.0	4.4	4.17	$0.0170 \pm 0.0021 \pm 0.0305$	4.17	$0.0604 \pm 0.0052 \pm 0.0469$
4.4	4.8	4.57	$0.0134 \pm 0.0027 \pm 0.0146$	4.57	$0.0271 \pm 0.0071 \pm 0.0232$
4.8	5.2	4.97	$0.0134 \pm 0.0029 \pm 0.0065$	4.97	$0.0277 \pm 0.0084 \pm 0.0132$
5.2	5.8	5.46	$0.0107 \pm 0.0027 \pm 0.0052$	5.49	$0.0163 \pm 0.0076 \pm 0.0082$
5.8	6.4	6.13	$0.0067 \pm 0.0008 \pm 0.0006$	6.13	$0.0121 \pm 0.0023 \pm 0.0011$
6.4	7.2	6.77	$0.0051 \pm 0.0005 \pm 0.0003$	6.77	$0.0114 \pm 0.0018 \pm 0.0009$
7.2	8.0	7.55	$0.0036 \pm 0.0006 \pm 0.0002$	7.55	$0.0044 \pm 0.0016 \pm 0.0003$
8.0	9.0	8.39	$0.0016 \pm 0.0006 \pm 0.0002$	8.38	$0.0053 \pm 0.0026 \pm 0.0004$
9.0	13.0	9.61	$0.0021 \pm 0.0013 \pm 0.0002$	9.58	$0.0030 \pm 0.0038 \pm 0.0003$

TABLE V. π^-/π^+ ratio vs p_t in p+Be and p+W collisions.

p_t range (GeV/c)		$< p_t >$ (GeV/c)	p+Be π^-/π^+	$< p_t >$ (GeV/c)	p+W π^-/π^+
4.0	4.4	4.18	$0.898 \pm 0.006 \pm 0.009$	4.18	$0.906 \pm 0.013 \pm 0.002$
4.4	4.8	4.58	$0.863 \pm 0.009 \pm 0.015$	4.58	$0.852 \pm 0.018 \pm 0.014$
4.8	5.2	4.99	$0.845 \pm 0.014 \pm 0.013$	4.99	$0.841 \pm 0.028 \pm 0.013$
5.2	5.8	5.47	$0.767 \pm 0.016 \pm 0.006$	5.47	$0.843 \pm 0.039 \pm 0.007$
5.8	6.4	6.07	$0.705 \pm 0.026 \pm 0.001$	6.07	$0.763 \pm 0.060 \pm 0.002$
6.4	7.2	6.75	$0.730 \pm 0.021 \pm 0.005$	6.75	$0.681 \pm 0.040 \pm 0.004$
7.2	8.0	7.56	$0.722 \pm 0.008 \pm 0.005$	7.55	$0.720 \pm 0.017 \pm 0.002$
8.0	9.0	8.43	$0.703 \pm 0.011 \pm 0.001$	8.43	$0.720 \pm 0.025 \pm 0.002$
9.0	10.0	9.44	$0.679 \pm 0.021 \pm 0.002$	9.43	$0.621 \pm 0.043 \pm 0.001$
10.0	13.0	11.00	$0.546 \pm 0.036 \pm 0.002$	10.99	$0.595 \pm 0.100 \pm 0.001$

TABLE VI. K^-/K^+ ratio vs p_t in p+Be and p+W collisions.

p_t range (GeV/c)		$< p_t >$ (GeV/c)	p+Be K^-/K^+	$< p_t >$ (GeV/c)	p+W K^-/K^+
4.0	4.4	4.18	$0.496 \pm 0.006 \pm 0.013$	4.18	$0.475 \pm 0.012 \pm 0.003$
4.4	4.8	4.58	$0.427 \pm 0.008 \pm 0.015$	4.58	$0.466 \pm 0.019 \pm 0.016$
4.8	5.2	4.99	$0.356 \pm 0.011 \pm 0.009$	4.99	$0.403 \pm 0.027 \pm 0.011$
5.2	5.8	5.47	$0.270 \pm 0.012 \pm 0.003$	5.47	$0.408 \pm 0.034 \pm 0.006$
5.8	6.4	6.07	$0.209 \pm 0.009 \pm 0.002$	6.07	$0.263 \pm 0.023 \pm 0.001$
6.4	7.2	6.75	$0.174 \pm 0.006 \pm 0.002$	6.75	$0.207 \pm 0.014 \pm 0.001$
7.2	8.0	7.56	$0.141 \pm 0.004 \pm 0.001$	7.55	$0.159 \pm 0.010 \pm 0.001$
8.0	9.0	8.43	$0.104 \pm 0.005 \pm 0.001$	8.43	$0.124 \pm 0.014 \pm 0.001$
9.0	13.0	10.19	$0.059 \pm 0.008 \pm 0.001$	10.17	$0.053 \pm 0.018 \pm 0.001$

TABLE VII. $\bar{p}/p$ ratio vs p_t in p+Be and p+W collisions.

p_t range (GeV/c)		$< p_t >$ (GeV/c)	p+Be $\bar{p}/p$	$< p_t >$ (GeV/c)	p+W $\bar{p}/p$
4.0	4.4	4.18	$0.050 \pm 0.006 \pm 0.091$	4.18	$0.121 \pm 0.011 \pm 0.093$
4.4	4.8	4.58	$0.051 \pm 0.011 \pm 0.086$	4.58	$0.064 \pm 0.017 \pm 0.062$
4.8	5.2	4.99	$0.052 \pm 0.012 \pm 0.022$	4.99	$0.073 \pm 0.023 \pm 0.030$
5.2	5.8	5.47	$0.061 \pm 0.016 \pm 0.025$	5.47	$0.051 \pm 0.024 \pm 0.023$
5.8	6.4	6.07	$0.056 \pm 0.007 \pm 0.003$	6.07	$0.070 \pm 0.014 \pm 0.004$
6.4	7.2	6.75	$0.045 \pm 0.005 \pm 0.001$	6.75	$0.066 \pm 0.012 \pm 0.004$
7.2	13.0	8.62	$0.028 \pm 0.004 \pm 0.003$	8.60	$0.032 \pm 0.009 \pm 0.002$

TABLE VIII. Particle fractions vs mass for p+Be$\rightarrow h^+ + h^-$.

Mass range (GeV/c^2)		$\pi^+\pi^-$ π^+K^- $\pi^+\bar{p}$	$K^+\pi^-$ K^+K^- $K^+\bar{p}$	$p\pi^-$ pK^- $p\bar{p}$
7.5	9.5	$0.518 \pm 0.002 \pm 0.022$	$0.229 \pm 0.002 \pm 0.012$	$0.105 \pm 0.002 \pm 0.020$
		$0.076 \pm 0.001 \pm 0.002$	$0.043 \pm 0.001 \pm 0.002$	$0.018 \pm 0.001 \pm 0.002$
		$0.002 \pm 0.001 \pm 0.007$	$0.001 \pm 0.001 \pm 0.003$	$0.008 \pm 0.001 \pm 0.009$
9.5	19.0	$0.561 \pm 0.002 \pm 0.013$	$0.248 \pm 0.002 \pm 0.007$	$0.085 \pm 0.002 \pm 0.014$
		$0.056 \pm 0.001 \pm 0.000$	$0.033 \pm 0.001 \pm 0.000$	$0.009 \pm 0.001 \pm 0.002$
		$0.003 \pm 0.001 \pm 0.000$	$0.002 \pm 0.001 \pm 0.001$	$0.002 \pm 0.001 \pm 0.004$

TABLE IX. Particle fractions vs mass for p+W$\rightarrow h^+ + h^-$.

Mass range (GeV/c^2)		$\pi^+\pi^-$ π^+K^- $\pi^+\bar{p}$	$K^+\pi^-$ K^+K^- $K^+\bar{p}$	$p\pi^-$ pK^- $p\bar{p}$
7.5	9.5	$0.480 \pm 0.005 \pm 0.023$	$0.223 \pm 0.005 \pm 0.014$	$0.116 \pm 0.005 \pm 0.022$
		$0.088 \pm 0.004 \pm 0.005$	$0.048 \pm 0.003 \pm 0.004$	$0.029 \pm 0.003 \pm 0.004$
		$0.005 \pm 0.003 \pm 0.011$	$0.005 \pm 0.003 \pm 0.006$	$0.006 \pm 0.003 \pm 0.009$
9.5	19.0	$0.555 \pm 0.007 \pm 0.017$	$0.245 \pm 0.007 \pm 0.007$	$0.101 \pm 0.006 \pm 0.016$
		$0.062 \pm 0.004 \pm 0.001$	$0.027 \pm 0.003 \pm 0.000$	$0.005 \pm 0.002 \pm 0.002$
		$0.004 \pm 0.002 \pm 0.005$	$0.001 \pm 0.001 \pm 0.001$	$0.000 \pm 0.003 \pm 0.001$

TABLE X. Species correlations vs mass for p+Be$\rightarrow h^+ + h^-$.

Mass range (GeV/c^2)		$\pi^+\pi^-$ π^+K^- $\pi^+\bar{p}$	$K^+\pi^-$ K^+K^- $K^+\bar{p}$	$p\pi^-$ pK^- $p\bar{p}$
7.5	9.5	$1.02 \pm 0.00 \pm 0.01$	$0.98 \pm 0.01 \pm 0.01$	$0.94 \pm 0.01 \pm 0.02$
		$0.93 \pm 0.01 \pm 0.02$	$1.16 \pm 0.02 \pm 0.02$	$1.02 \pm 0.05 \pm 0.12$
		$0.28 \pm 0.49 \pm 0.20$	$0.36 \pm 0.60 \pm 0.22$	$5.60 \pm 0.12 \pm 1.60$
9.5	19.0	$1.01 \pm 0.00 \pm 0.00$	$0.98 \pm 0.01 \pm 0.00$	$0.99 \pm 0.01 \pm 0.02$
		$0.92 \pm 0.02 \pm 0.01$	$1.19 \pm 0.03 \pm 0.01$	$0.95 \pm 0.09 \pm 0.05$
		$0.72 \pm 0.19 \pm 0.26$	$0.83 \pm 0.33 \pm 0.25$	$3.30 \pm 0.30 \pm 1.29$

TABLE XI. Species correlations vs mass for p+W$\rightarrow h^+ + h^-$.

Mass range (GeV/c^2)		$\pi^+\pi^-$ π^+K^- $\pi^+\bar{p}$	$K^+\pi^-$ K^+K^- $K^+\bar{p}$	$p\pi^-$ pK^- $p\bar{p}$
7.5	9.5	$1.02 \pm 0.01 \pm 0.01$	$0.99 \pm 0.02 \pm 0.00$	$0.93 \pm 0.03 \pm 0.01$
		$0.93 \pm 0.03 \pm 0.01$	$1.05 \pm 0.05 \pm 0.01$	$1.17 \pm 0.09 \pm 0.07$
		$0.53 \pm 0.52 \pm 0.11$	$1.05 \pm 0.55 \pm 0.14$	$2.70 \pm 0.42 \pm 0.94$
9.5	19.0	$0.99 \pm 0.01 \pm 0.00$	$1.00 \pm 0.02 \pm 0.00$	$1.05 \pm 0.03 \pm 0.01$
		$1.05 \pm 0.04 \pm 0.00$	$1.06 \pm 0.09 \pm 0.01$	$0.53 \pm 0.39 \pm 0.05$
		$1.29 \pm 0.58 \pm 0.14$	$0.64 \pm 1.06 \pm 0.36$	$0.23 \pm 21.55 \pm 0.57$

ative hadron species β is defined in terms of the particle fractions $f_{\mu\nu}$ where $\mu = \pi^+, K^+, p$ and $\nu = \pi^-, K^-, \bar{p}$ as

$$c_{\alpha\beta} = \frac{f_{\alpha\beta}}{(\sum_\nu f_{\alpha\nu})(\sum_\mu f_{\mu\beta})}. \quad (5)$$

Tables X and XI give the opposite-side correlations for each pair species produced in p-Be and p-W collisions. A statistically significant correlation between opposite-side K^+ and K^- is seen in the p-Be data. If strangeness is strongly enhanced in gluon fragmentation, then the observed K^+K^- correlation could reflect a parton-level gluon-gluon correlation arising from the large gluon-gluon scattering amplitude. Both targets show a strong correlation between protons and antiprotons, though with large systematic errors. The large $p\bar{p}$ correlation could reflect a correlation between high-p_t diquarks and opposite-side high-p_t gluons arising from a large gluon-diquark scattering amplitude. It may be that parton-level correlations are insufficent to explain the observed correlations. If that is true, then these final-state correlations indicate that, at high-z, compensation of strangeness and baryon number can occur between hadrons very far apart in momentum.

ACKNOWLEDGMENTS

This work was supported in part by the U.S. Department of Energy, the National Science Foundation, the Commisariat à l'Energie Atomique, and the Japan Ministry of Education, Science and Culture (Monbusho).

[1] H. Aihara *et al.*, Phys. Rev. Lett. **61**, 1263 (1988).
[2] A.L.S. Angelis *et al.*, Nucl. Phys. **B209**, 284 (1982).
[3] J.A. Crittenden *et al.*, Phys. Rev. D **34**, 2584 (1986).
[4] D.E. Jaffe *et al.*, Phys. Rev. D **40**, 2777 (1989).
[5] P.B. Straub *et al.*, Phys. Rev. Lett. **68**, 452 (1992).
[6] M. Adams *et al.*, Nucl. Instrum. Methods **217**, 237 (1983).
[7] R. McCarthy *et al.*, Nucl. Instrum. Methods **A248**, 69 (1986).
[8] R. Bouclier *et al.*, Nucl. Instrum. Methods **205**, 403 (1983).
[9] Ph. Mangeot *et al.*, Nucl. Instrum. Methods **216**, 79 (1983).
[10] P.B. Straub, Ph.D. thesis, University of Washington, 1990.
[11] The low probability of reinteraction in the 14% interaction length targets was possible because secondaries exited through the top or bottom of the thin targets, not out the back.
[12] D. Antreasyan *et al.*, Phys. Rev. D **19**, 764 (1979).
[13] D. Antreasyan *et al.*, Phys. Rev. Lett. **38**, 115 (1977).
[14] A. Breakstone *et al.*, Phys. Lett. **135B**, 510 (1984).
[15] S. Ekelin and S. Fredriksson, Phys. Lett. **149B**, 509 (1984).
[16] A. Breakstone *et al.*, Z. Phys. C **28**, 335 (1985).